Super-Coiling of DNA Plasmids: Mechanics of the Generalised Ply

J. M. T. Thompson, G. H. M. van der Heijden & S. Neukirch

Centre for Nonlinear Dynamics, Civil Engineering Building,
University College London, Gower Street, London, WC1E 6BT

(Revised version for Proc. R. Soc. Lond., Series A, 07/08/01)

Abstract

In this paper we address the mechanics of ply formation in DNA supercoils. We extend the variable ply formulation of Coleman and Swigon to include end loads, and the derived constitutive relations of this generalised ply are shown to be in excellent agreement with experiments. We make a careful physical examination of the uniform ply in which two strands coil around one another in the form of a helix. We next address the problem of determining the link (*Lk*), twist (*Tw*) and writhe (*Wr*) of a closed DNA plasmid from an inspection of its electron micrograph. Previous work has made use of the topological relation, $Lk = Tw + Wr$, but we show how this *kinematic* result can be augmented by the *mechanics* solutions. A very precise result is achieved in a trial calculation.

1. Introduction

Spatial deformations of the DNA molecule are central to its biological functioning. To transcribe the genetic code, DNA must screw 'through' an RNA polymerase. This involves a rotation at about 10 turns per second which can induce large twisting stresses in the DNA. The double-helix of most DNA molecules is right-handed, and if this intrinsic internal twist is increased by stress the molecule is said to be *overwound*: conversely, it is *underwound*. If DNA becomes excessively twisted or knotted, it is unable to function, and to overcome this the body has a de-knotting enzyme, the *topoisomerase*. This remarkable enzyme can cut the molecule, untwist it to alleviate the stress, and re-join it. This un-knotting is so vital, that some anti-cancer drugs aim to poison the enzyme: by disabling the topoisomerase, they stop cancer cells from growing out of control.

Many significant deformation phenomena operate on a scale at which the internal double-helix of the DNA is irrelevant, and a long strand behaves as if it were a slender elastic rod or fibre. The length scales involved are nicely described by Calladine & Drew (1997), who point out that if a DNA molecule were magnified a million times it would have the thickness of a kite string, and would stretch from London to Cambridge ($\approx$ 100 km). There is, indeed, an explosion of research by biologists and mathematicians on the mechanics of a long elastic fibre modelling a single DNA molecule. See for example: Stump *et al* 1998, Swigon 1999, Tobias *et al* 2000, Coleman *et al* 2000, Stump & Fraser 2000, Coleman & Swigon 2000. The results can be of great help to molecular biologists in understanding and controlling the spatial writhing of a molecule.

One topic that is attracting attention is the super-coiling of DNA, in which the long fibre representing the double helix adopts a configuration such as that illustrated in fig 1. This shows a silicone rubber rod forming a left-handed variable balanced ply (*VBP*) with one free end loop. The helical angle varies along the ply, and at the un-looped end there is a visible separation followed by a discrete point contact. This *VBP-skip-fly* phenomenon was discovered by Coleman and Swigon (2000).

The interwound configuration of this rubber rod is said to form a *ply*. The simplest way to observe a ply physically is to twist a long rubber rod of circular cross-section. If, after imposing the twist, the ends are brought together, the rod will buckle locally and jump into this familiar ply-plus-loop form. Extensive experimental and theoretical studies of the initial buckling and localised post-buckling, prior to self-contact, have been made by the present authors and others (Thompson & Champneys 1996, Champneys & Thompson 1996, Champneys *et al* 1997, van der Heijden & Thompson 1998, van der Heijden *et al* 1998, Goriely & Tabor 1998). This work uses the static- dynamic analogy, and has covered rods of circular and non-circular cross-section. Meanwhile the symmetry and bifurcation properties of closed but non-contacting rods have been studied extensively by Maddocks and co-workers: see for example Manning & Maddocks (1999).

A molecule of DNA often forms a closed loop, called a *plasmid*. An electron micrograph of a plasmid, reproduced by Calladine & Drew (1997), shows negatively supercoiled, interwound DNA as prepared from *E. coli* bacteria. Four ply-plus-loop regimes are clearly visible in this micrograph (the sketch is purely notional, and cannot be used for link or writhe estimates). A basic configuration of a twisted plasmid, derived analytically from elastic rod theory by Coleman & Swigon (2000), is shown in fig 2: we discuss this picture in section §9. A straight central region forms a left-handed variable ply, closed by two free end loops. Under such conditions the ply is described as *balanced*: conversely, if the loops carry forces or moments, we call it *loaded*.

The paper is organised as follows. Section §2 discusses the modelling of plies, §3 introduces the kinematics of link, twist and writhe, and §4 describes how an experimental ply can be made. In §5 we present our direct mechanical formulation of the variable-angle loaded ply, and its specialisations. In §6 we examine solutions of the variable balanced ply: §6.1 gives a phase-space view, §6.2 summarises plasmid solutions of Coleman & Swigon (2000), §6.3 covers related work on a wrench-loaded rod. Section §7 is devoted to the solution of the uniform balanced ply: while §8 looks at the uniform loaded ply with an energy formulation, derived constitutive relationships, and experimental verification. In §9 we show that our mechanics results can determine writhing characteristics from a DNA micrograph. After concluding remarks in §10, Appendix 1 gives our principal notations and Appendix 2 sketches a new variational formulation of the generalised ply.

2. Modelling of a ply

In analysing the mechanics of ply formation, a DNA molecule can be regarded as an elastic rod with circular cross-section of radius r. This rod can usually be treated as homogeneous, inextensional, and (linearly) elastic in response. All we then need to know about its mechanical properties is the ratio, g , of its torsional stiffness, C, to its bending stiffness, B. Molecular biologists have made many experiments to estimate g , and it is thought to lie in the interval $0.7<g<1.5$. See Horowitz & Wang (1984), Bouchiat & Mezard (1998), Strick, *et al* (1996), Heath, *et al* (1996). A comparison of discrete and continuum modelling is made by Manning, *et al*, (1996): a continuum rod model with intrinsic curvature is fitted to experimentally motivated base-pair-level discrete DNA models. Equilibrium energies of closed rings predicted by the continuum model match those of the underlying discrete model to within 0.5 %. A discussion of possible nonlinear coupling between the bending and twisting of DNA is given by Calladine (1980).

Now for laboratory experiments we might want to model a strand of DNA with a solid

circular rod of metal or rubber. For such a rod we have $\gamma = C/B = 1/(1+\nu)$, where ν is Poisson's ratio of the material. Typically, for a metal rod engineers take $\nu = 1/3$, giving $\gamma = 3/4$, while for a rubber rod they take $\nu = 1/2$, giving $\gamma = 2/3$. At the bottom end of the biological range we have $\gamma = 0.7$ corresponding to $\nu \approx 0.43$, while at the top end we have $\gamma = 1.5$, $\nu = -1/3$. This negative value of ν is not observed for any normal material.

Two major contributions to our understanding of the mechanics of a ply have been made recently. First, Fraser and co-workers (Fraser & Stump 1998, Stump *et al* 1998) derived the equation of a *uniform balanced ply* (*UBP*). This has two segments of rod winding around themselves, and touching each other on a straight central line, the *ply axis*. Conditions are assumed to be uniform along the unloaded ply, so the centre line of a segment forms a helix of radius r and constant helical angle θ. This solution will only be observed if the correct boundary conditions are applied at the ends, and will not be observed in a ply bounded by free end loops. It may however hold approximately in the central region of a very long ply between 'boundary layers' in which θ adjusts to allow separation (into, for example, a loop).

Second, Coleman & Swigon (2000) derived the equation of a *variable balanced ply*, which allows θ to vary, with the two segments lying as if wound on a cylinder of radius r. Any finite-length ply between free end loops will always have a variable θ, and it is the extra flexibility of the variable ply that allows the rods to separate at the ends without the unphysical point moment that had to be introduced by Fraser and his co-workers.

In the present paper, we relax the condition of balance, and present the equations of a *variable loaded ply* (*VLP*) which we might refer to more simply as a *generalized ply* (*GP*). This carries a wrench, comprising a tensile force, G, and a twisting moment N acting about the tension axis. This *GP* can exist under a wide range of end conditions, and is easily specialised to either of the previous two cases when $G = N = 0$. Note that this *GP* solution arises as a special case of a general study of a rod constrained to lie on a cylinder (van der Heijden, 2001): all that is required is to set the radius of the cylinder to r. For asymmetric rods on a cylinder see van der Heijden, Champneys & Thompson (2002). Here, however, we give a direct physical derivation that throws much extra light on the mechanics and will be of particular value to biologists who do not have a background in continuum mechanics. We examine the predicted constitutive relations of the ply, and show them to be in good agreement with a new experimental result.

3. Topology of Link, Twist and Writhe

3.1 The striped rod

Before studying the mechanics of a ply, we need a clear understanding of the kinematics involved. Consider an initially straight elastic rod of circular cross-section, with length L and radius r. We imagine the rod to be axially inextensional, so its length L will never vary. While the rod is straight and unstressed, we imagine parallel lines to be painted on its surface, parallel to its straight centre-line. We refer to this as our *striped rod*.

3.2 The kinematic twist rate

While it remains straight, we imagine the striped rod to be twisted uniformly by applying a rotation about the centre-line, ϕ, (in radians) to one end while the other end is held fixed. The kinematic twist rate is then defined as $\tau \equiv \phi / L$, taken to be positive if the stripes on

the surface form a *right-handed helix*. The stripes then look like a normal screw thread, and the vector arrows representing t on the end of a rod point outwards (like tension). Imagining the cylindrical surface of the twisted rod to be unrolled, the planar *stripe angle*, y , between the helical stripes and the centre-line is in many ways a more convenient measure of the twist rate than t , and we note that they are related precisely by

$$\tan y = t\, r \tag{1}$$

We take this as our definition of y, noting however that it will not be the unrolled angle of the stripes on a bent rod. The outer tensile fibre of a rod whose centre line is bend into a circle of radius *R* has, by similar triangles, a strain (elongation/length) equal to *r*/*R*: and if the centre-line of the rod lies on a cylinder of radius *r* with helical angle q we have $R = r / \sin^2 q$. So the strain is $\sin^2 q$, and rather than (1) the angle will be given by $\tan y = t\, r/(1 \pm \sin^2 q)$, the plus sign for the tensile face, the minus sign for the compressive face. These differences can be appreciable. The total twist in the rod, *Tw*, (measured not in radians but in complete turns) is the integral of $t / 2p$ over *L*, which for constant t gives

$$Tw = t\, L / 2\, p\, . \tag{2}$$

The sign convention for *Tw* follows naturally from that of t.

3.3 Link and Writhe

To introduce the topological concepts of link and writhe, we imagine gluing the two ends of our striped rod together to form a closed loop. If we just bend the rod in a plane and glue the ends together without inserting any twist, it will adopt a circular shape, and the stripes will all be circles. Suppose, however, that having bent it in a plane and brought the ends together we insert, at the last minute, a number of full turns of twist just before gluing. We define this number as the link, *Lk*, taken to be positive if it induces positive t in the planar ring. For as long as the glued ring remains planar, we have *Lk* = *Tw*.

Strictly, the link of a plasmid will vary by integer increments because each sugar-phosphate chain of the double helix must join to itself: and in mathematical topology the link is also normally taken to be integer. However, in the context of elastic rod theory (where the ends of a rod can be glued together at any angle) it is convenient to ignore this technicality and speak as if *Lk* varies continuously.

Now *Lk* is a topological invariant. If we get hold of the glued ring and distort it, in or out of the plane, in any way we choose, the link will not change. The total twist does however change, and the two are related by the important result (see for example: Calugareanu, 1961; White, 1969; Fuller, 1971),

$$Lk = Tw + Wr \tag{3}$$

The writhe, *Wr*, is just a property of the shape of the rod's centre-line, defined as follows.

3.4 Directional writhe and signed crossings

The writhe is perhaps best introduced as the number of (signed) crossings in a view, averaged over all views (Fuller, 1971). The number of crossings in a single view is called the directional writhe, *Dr* : in the particular side view of fig 2, for example, a count of the

number of crossings gives $Dr = 8$. In general, in calculating Dr, we must take the number of *signed* crossings, according to the right-hand rule explained in fig 3. Averaging over all views we then obtain

$$Wr = < Dr > \qquad (4)$$

4. Making an experimental ply

4.1 A ply from two straight rods

To conclude our discussion of kinematics, it is necessary to consider how we propose to make a ply, either conceptually or in an actual laboratory experiment. To make a *right-handed* ply, we take two identical rubber rods of circular cross-section, each of length L, as illustrated in fig 4. Both are initially straight, and they are laid side by side on a bench with their left-hand ends fixed. While remaining straight, each rod is given a left-handed twist by turning the right-hand ends through a positive angle A, anti-clockwise when looking down the rod from left to right. Since our convention for twist is right-handed, this makes our initial rate, t_0, numerically equal to $-A/L$.

We *define* this straight twisted configuration as the a-state of the ply. The stripe angle, y, is given by (1), and we write its initial value as y_a with $\tan y_a = t_0 r$. To make a fairly uniform ply, angle A should correspond to at least 5 complete turns. The rods are now joined together at both ends. For a demonstration they can be clipped together with a paper clip, or wrapped together with tape. For an experiment, we can cast the ends together in a moulding. Thinking of these two straight, planar rods and their mouldings as one closed entity, the writhe is zero, and (2), (3), give $Lk = t_0 2L/2p$. This invariant link (which will be at least 10) will be preserved when we release the rods from the bench, and load the resulting ply.

Before release, the straight rods already form an example of our loaded ply, because the resultant applied constraint is simply a twisting moment, $N = 2Ct_0$, with zero tension ($G = 0$). In fact, when we leave go of the rods (still clipped together at their ends) they might jump into a variety of spatial forms, one of which will be a *right-handed* balanced ply, with approximately constant q. A controlled way to get this ply would be to hold the two clips, and just let them rotate slowly about the ply axis until the ply reaches equilibrium under zero wrench. We can finally load this ply by applying any wrench, (G, N), to the mouldings. Notice that once the rods are released, the moulding will not provide the correct end conditions for a uniform ply, but we can expect any significant non-uniformity to be localised near the ends (as confirmed in fig 12).

4.2 A ply from a single rod

An alternative way to make the ply would be to start with a single straight rod of length just over $2L$. After putting in a twist rate t_0 while straight, we glue the 2 ends to form a plane circle with $Wr = 0$, $Lk = t_0 L/p$. With Lk greater than 10, the released circle will normally form a balanced ply with two end loops: though other equilibrium shapes may be possible. We can finally imagine the end loops to be cast in a mould, to give roughly the same as in §4.1, with the excess length taken up by the end loops.

4.3 Kinematics of ply manufacture

In terms of the current angle q, assumed constant, we now need to write down the writhe of the two helical rods of §4.1. To do this we use the result of Fuller (1978) that for a single rod $1 + Wr$ = area/$2p$ (mod 2). Here the area is that enclosed, cumulatively, by the orbit of the unit tangent vector on the unit sphere. Application of this result, as in van der Heijden & Thompson (2000) gives immediately their eqn (65), which for our two-strand ply becomes

$$Wr = K(1- \cos q) - K(1 + \cos q) = - L \sin 2q /2p r \qquad (5)$$

where K is the number of helical waves in one rod given by $K = L \sin q /2p r$. With the conservation of link, (3) now gives us

$$Lk\,(p\, r/L) = t_0 r = \tan y_a = t\, r - ½ \sin 2q = \tan y - ½ \sin 2q \qquad (6)$$

For small angles, this simplifies to $q \approx y - y_a$. The kinematic equation (6) relates the given initial twist rate, t_0, to the final current twist rate, t, and will be needed to allow completion of our uniform ply studies. It was noticeably absent from the paper of Fraser & Stump (1998) who used instead an energy balance which would not apply in the present circumstances.

5. Mechanics of the generalised ply

From now on we shall use the word *ply* to mean two segments of rod in continuous contact along a straight *ply axis*, and winding around this axis in a symmetric way: rotation of the ply about its axis through 180° leaves the picture unchanged. By the *end* of the ply we mean the point at which the continuous line contact ceases. Coleman and Swigon (2000) have shown that this end point requires very careful consideration.

5.1 Geometry of the ply

We give here a direct and self-contained physical analysis of the *generalised ply*, illustrated in fig 5. This shows a horizontal *right-hand ply* from the side. Each circular rod of radius r, bending stiffness B and torsional stiffness C, lies as if its centre-line were wound on a cylinder of radius r : in the special case of a *uniform ply*, each rod would have the form of a helix. A moulding surrounding the end loop is imagined to be loaded by tension G and twisting moment, N, the latter tending to tighten the mutual winding of the rods. We ignore friction and gravity, and write the variable ply angle as $q(s)$ where s is the distance along the centre-line of either rod. We denote the straight central axis of the ply, on which the two rods touch, by **Ax**, and focus on the section, **Se**, where, in our view, the rod centre-lines cross. The front rod, **Fr**, nearest the eye, slopes down to the right at angle q to **Ax**, while the rear rod slopes up to the right at the same angle. We use **Pa** to denote any plane that is parallel to the plane of the paper.

5.2 Force balance for the ply

We imagine the rods cut, at right angles to their own centre-lines, at **Se**. On the rods to

the left of **Se** transmitted from the rods to the right are: a tension, T, along each rod axis, lying in **Pa**; a shear force, V, normal to each rod axis, lying in **Pa** with the sign convention of the diagram; a shear force, U, normal to T and V, acting into the paper on **Fr**. The vector sum of T and V is decomposed into a force F, normal to **Ax**, and a force ½ G along **Ax**, the latter ensuring the horizontal force balance of the ply to the left of **Se** and including the loaded end loop. The equations of decomposition are

$$V = F \cos q - \tfrac{1}{2} G \sin q \tag{7}$$

$$T = F \sin q + \tfrac{1}{2} G \cos q \tag{8}$$

5.3 Moment balance for the ply

The transmitted moments are: twisting moment in a rod, Ct , with vector along the T vector; bending moment, M_P, with vector along the $-V$ vector; and a bending moment M_N, with vector into the paper on **Fr**. We write the bending moments in terms of the equivalent rod curvatures as $M_P = B \sin^2 q / r$ (this exact curvature multiplying B is also that of a helix of constant q) and $M_N = B q'$ where a prime denotes differentiation with respect to s (this exact curvature looks intuitive in **Pa**). The moment balance for the ply and loaded end loop for twisting about **Ax** is

$$Ct \cos q + M_P \sin q + Fr = \tfrac{1}{2} N \tag{9}$$

Using (7) and our expression for M_P, equation (9) becomes

$$Vr^2 = - Ct\, r \cos^2 q - B \sin^3 q \cos q - \tfrac{1}{2} Gr^2 \sin q + \tfrac{1}{2} Nr \cos q \tag{10}$$

5.4 Force balance for a rod element

We now look at the equilibrium of an element of rod **Fr** of length δs, starting (say) at section **Se**, as drawn. Balancing forces in the plane normal to **Ax** introduces the contact pressure force $p\, \delta s$, where we should note that p is the force per unit distance along the centre-line of one of the rods (not, per unit distance along **Ax**). Now there are 3 force components acting across a section of the rod, T, V, U, and the first two have been replaced by F, G. Since G is parallel to **Ax**, we are just left with F and U, both of which lie in the plane normal to **Ax**. Resolving in this plane along $p\, \delta s$ gives $p\delta s = \delta U + F\, \delta a$, from which we obtain $p = U' + (F/r) \sin q$. Resolving at right-angles to $p\delta s$ gives $\delta F = U\, \delta a$, from which we have $F' = (U/r) \sin q$. Note that for a uniform ply, with all derivatives zero, we have $U = 0$ and $pr = F \sin q$. We do not need the formulae of this section for the present analysis, but we use of them in later studies of the uniform plies.

5.5 Moment balance for a rod element

Taking moments for a rod element about its own centre-line shows immediately that the twist rate, t , remains constant along the rod. We next write down the clockwise moments on the element about an axis out of **Pa**. The forces T and V, give the moment $+ V\, \delta s$. Vector M_P is decomposed into $M_F = M_P \cos q$ in the direction of $-F$, and M_A which plays no part. So from M_P we have $- M_F\, \delta l = - B\, \delta s \sin^3 q \cos q / r^2$. Twisting moment Ct enters by

virtue of the curvature $\sin^2\theta / r$ giving $+C\tau\ \delta s \sin^2\theta /r$. Finally, including $+\delta M_N = +B\theta'^2\ \delta s$, and multiplying through by r^2, we have the balance condition

$$Vr^2 + B\theta'^2 r^2 = B \sin^3\theta\ \cos\theta\ - C\tau\ r\ \sin^2\theta \qquad (11)$$

Eliminating V by subtracting (10) from (11), and setting $C/B = \gamma$, we have

$$\theta'^2 r^2 = 2 \sin^3\theta \cos\theta + \tau\ r\gamma\ \cos 2\theta + \tfrac{1}{2}(Gr^2/B) \sin\theta - \tfrac{1}{2}(Nr/B) \cos\theta \qquad (12)$$

as derived by van der Heijden (2001). Notice that this is a differential equation for the variation of $\theta(s)$ along a rod of the ply.

5.6 Specialisation to the variable balanced ply

With no end loads, we have $G = N = 0$, and equation (12) for $\theta(s)$ becomes

$$\theta'^2 r^2 = 2 \sin^3\theta \cos\theta + \tau\ r\ \gamma\ \cos 2\theta \qquad (13)$$

agreeing with eqn (2.41) of Coleman & Swigon (2000) if we replace our τ by their $\Delta\Omega$.

5.7 Specialisation to the uniform balanced ply

Setting $G = N = \theta'' = 0$ retrieves the *uniform balanced ply* of Fraser & Stump (1998) and Stump *et al* (1998), for which the twist rate is given by

$$\tau\ r\ \gamma\ =\ \gamma\ \tan\psi_\beta\ =\ -\sin^2\beta\ \tan 2\beta \qquad (14)$$

We *define* this uniform balanced condition as the β-state of the ply, and write the stripe angle as ψ_β and the helical angle as β. For small angles this simplifies to

$$\tau\ r\ \gamma\ \approx \gamma\ \psi_\beta\ \approx\ -2\beta^3 \qquad (15)$$

In (14) the negative sign tells us that the current twist rate, τ, is *negative* in the present *right-hand ply*, as is the initial twist rate, τ_0. In general when we make a ply and pass from the α-state to the β-state we observe:

The twist rate is reduced in magnitude, but does not change its sign

The helical angle of the ply has the opposite sign to the twist rates

The twists have the opposite sign to the space torsion of the helix

The β-state corresponds to a fixed point of the differential equation (13), as we shall examine in section §6. Looking back through the generalised ply analysis, we retrieve the following results for the forces in the uniform balanced ply,

$$\gamma\ \tau\ r\ = -2Vr^2/B = -\ \sin^2\beta\ \tan 2\beta \qquad)$$

$$T = p\,r = V \tan\beta \qquad (16)$$

The two following versions of Vr^2 from (11) and (10) respectively look superficially incompatible, and can cause confusion: they are easily proved equal using (12):

$$Vr^2 = \tfrac{1}{2} B \sin^2\beta\,(\sin 2\beta - 2\gamma\tau\, r) = -B\cos\beta\,(\sin^3\beta + \gamma\tau\, r\cos\beta) \qquad (17)$$

These results from the mechanics analysis agree with those in equation (3.5) of Stump *et al* (1998), after a few sign changes due to different conventions. Notice that τ, V, T, p all tend to infinity as β tends to 45° due to the tan 2β in (16). In fact 45° is the lock-up angle, as we discuss in §7.3.

5.8 Specialisation to the uniform loaded ply

Setting just $\theta'' = 0$ in (12) gives us the equation of the *uniform loaded ply* (*ULP*) whose constitutive relations we shall examine later,

$$2\sin^3\theta\cos\theta + \tau\, r\gamma\cos 2\theta + \tfrac{1}{2}(Gr^2/B)\sin\theta - \tfrac{1}{2}(Nr/B)\cos\theta = 0 \qquad (18)$$

6. Solutions of the variable balanced ply

6.1 Phase portrait

It is useful to employ the static-dynamic analogy, and examine the solutions of the differential equation (13) in the phase space obtained by replacing arc length s by time t. In thinking about this equation we should note that the current twist rate, τ, is constant along a rod, having been shown to be not a function of s. We do not need its magnitude for the present discussion: but we note that we could find it in terms of the initial τ_0 using a suitable generalisation of (5) and (6) to conditions of variable θ. Equating s to a notional t gives us, then, an equivalent undamped nonlinear oscillator which has the phase portrait shown in fig 6. The saddle point (S) of this oscillator with $\theta = \beta$, found by setting $\theta'' = 0$, is of just the *UBP* of (14).

The uniform ply will only exist if the correct boundary conditions are applied at the ends. In general this will not be the case, as when the ply is closed by end loops. However, a long (symmetric) ply will often have $\theta(s) \approx \beta$ over a long central section. In phase space, this will correspond to a solution close to S, with small θ'. The divergence before and after the slow transit near S gives a 'boundary layer' in which $\theta(s)$ adjusts relatively quickly to accommodate the conditions at the end of the ply (see fig 12). To illustrate this, we give an over-view of the ply-loop solutions of Coleman & Swigon (2000).

6.2 Writhing of twisted plasmids

Using their variable ply results, and sophisticated analytical techniques, Coleman & Swigon (2000) have studied the writhing of a DNA plasmid, modelled as an initially straight elastic rod of circular cross-section (fig 7). The ends of the rod are imagined to be glued together after a number of complete turns of twist have been inserted. We shall refer to this number as the link, *Lk*, noting however that Coleman and Swigon call it the excess

link because they use a datum that includes the twisting of the double helix itself. For a given controlled input of *Lk* they calculate the spatial equilibrium configuration of the plasmid, taking full account of all (frictionless) self-contacts. As their measure of deformation they adopt the writhe, *Wr*, which is the measure of the spatial shape of the rod's centre line that we outlined earlier.

The response under slowly varied *Lk* is shown in the left-hand picture of fig 7. The rod is stable in its planar circular state up to the subcritical bifurcation at A^0, from which a dynamic jump would carry the ring to a state of self-contact as illustrated by the double arrow. The bifurcation at A^0 is at

$$Lk = (B/C)\sqrt{3}, \tag{19}$$

a result due to Zajac (1962). Ignoring for the moment the physical jumping behaviour, it is useful to focus on the post-buckling path that emerges from A^0, noting as we go that the number of self-contact points is shown in square brackets: and a solid (or broken) line denotes a stable (or unstable) path under controlled *Lk*.

Between A^0 and A^1 we have an unstable falling path with no self-contact. Between A^1 and A^2 we have a path with one self-contact at a point; between A^2 and A^3 a path with self-contact at two points; and between A^3 and A^4 a path with self-contact at three points. After A^4 a continuous line of self-contact, namely a ply, is observed, together with self-contact at two points. The jumps that would be encountered under slowly varying *Lk* are indicated, and sample computed shapes are superimposed. An experiment that we have performed on a metal rod confirms the predicted sequence of jumps and contacts.

The right-hand diagram of fig 7 shows details of the self-contacts as we progress along the post-buckling path $A^0\ A^1\ A^2\ A^3\ A^4\ \ldots$. We see that a single central point-contact splits into two at A^2, followed by a new central point-contact at A^3. At A^4 this central point-contact starts to spread to give us finally a central symmetric ply, which *skips* off at each end, only to re-contact at a point shortly after, before the two rods finally *fly* apart. Fig 1 shows a variable ply with lift-off and re-contact. The continuation of the *Lk* versus *Wr* graph to higher values is shown in fig 8. Also shown as a function of *Wr* is the central winding angle, $q(0)$, and the range of angle encountered in the ply. Notice that the latter is very small, implying that the ply is very nearly uniform. We return to some of the predicted rod shapes in §9.

Coleman *et al* (2000) have also found co-existing stable states of self-contacting plasmids, and have evaluated the transition energies (at the mountain passes corresponding to unstable states) needed to get from one stable state to another. This useful information governs the thermodynamic probability of observing a stable equilibrium state. They have also analysed the physical shapes of knotted plasmids (Swigon 1999).

6.3 Looping and ply formation of a stretched and twisted rod

Somewhat analogous to the writhing of a closed plasmid is the response of a single stretched and twisted rod. If the rod is regarded as infinitely long, its behaviour before self-contact can be studied by the use of the static-dynamic analogy in which the arc-length of the static rod is identified as time in an equivalent dynamical system. Specifically, deformations of a rod of symmetric (or non-symmetric) cross-section are equivalent to the motions of a symmetric (or non-symmetric) spinning top. The integrable symmetric case

admits closed form solutions, while the non-integrable non-symmetric case can exhibit chaos (Thompson & Champneys 1996, Champneys & Thompson 1996, Champneys *et al* 1997, van der Heijden & Thompson 1998, van der Heijden *et al* 1998, Goriely & Tabor 1998).

Calculations for a finite-length pin-ended rod with self-contact are given by Swigon (1999). Regarding the axial tension, T, as fixed, with the applied end rotation as a slowly varying control, dynamic jumps and contact regions are similar to those of the plasmids. The bifurcation at A^0 is now given by the Greenhill formula,

$$Lk = (B/C)\sqrt{[1 + (TL^2/B\pi^2)]}. \tag{20}$$

The general pattern of the predicted response has been observed in simple trial experiments in our laboratory. New theoretical and experimental work on the finite-length, stretched and twisted rod with camped ends (van der Heijden, et al, 2002) includes a numerical study of the successive discrete self-contacts and jump phenomena.

7. Solution of the uniform balanced ply

7.1 Prediction of the ply angle

The final solution for the right-handed *UBP* is obtained by eliminating t between the kinematic equation (6) and the mechanics equation (14) to give

$$\tan \psi_a = t_0 r = -\tfrac{1}{2} \tan 2\beta \, (1 + 2\nu \sin^2 \beta) \tag{21}$$

where ψ_a is the initial helical angle of the stripes and β is the balanced solution for α. For convenience, we have replaced the stiffness ratio, γ, by Poisson's ratio using $\gamma = 1/(1+\nu)$. If we plot the given $t_0 r$ against the produced ply angle β we see that $t_0 r$ goes to infinity as β approaches 45°. For small angles, (21) simplifies to

$$\psi_a \approx -\beta \tag{22}$$

Setting $\alpha = \beta$ and $\psi = \psi_b$ (stripe angle in the β-state) in the approximation of (6) gives us $\psi_b \approx 0$. So, to this first order, as we go from the α-state to the β-state we have:

The stripe angle vanishes and is converted into a ply angle of the opposite sign

7.2 The link versus writhe diagram

It is useful to write down some results in terms of the double angle and ν. Using (6) and (21) we obtain the link, using (2) and (14) the twist (for two rods of length L), and using (5) the writhe as follows

$$Lk\,(2\pi r/L) = \nu \sin 2\beta - (1+\nu) \tan 2\beta \tag{23}$$

$$Tw\,(2\pi\, r/L) \;=\; (1+\nu)(\sin 2\beta - \tan 2\beta) \tag{24}$$

$$Wr\,(2\pi\, r/L) \;=\; -\sin 2\beta \tag{25}$$

We notice that the writhe takes its maximum numerical value of $Wr^* = L/2\pi\, r$ at $\beta = 45°$. First order solutions for small angles are

$$Lk\,(2\pi\, r/L) \;=\; -2\beta \tag{26}$$

$$Tw\,(2\pi\, r/L) \;=\; -4(1+\nu)\,\beta^{3} \tag{27}$$

$$Wr\,(2\pi\, r/L) \;=\; -2\beta \tag{28}$$

showing that within this approximation the twist is of smaller order than the link and writhe: all the total twist of the straight rods has been converted into writhe. The energy aspects of this conversion are summarised later in §8.3. If we eliminate β between (23) and (25) we obtain the relation between link and writhe

$$Lk \;=\; Wr\,\{-\nu \;+ (1+\nu)\,/\sqrt{\,[1 - (Wr/Wr^*)^2\,]}\} \tag{29}$$

This gives a graph for our manufactured ply which can be compared with the diagram of Coleman and Swigon for a plasmid, as illustrated in fig 9.

7.3 The lock-up angle

Just as $\tau_0 r$ goes to infinity as β tends to 45°, so do the internal forces and moments, τ, V, T and p. Although apparently unrelated, we note that $\beta = 45°$ is in fact the geometrical lock-up angle at which a ply self-contacts, making $\beta > 45°$ kinematically impossible. Analyses of this geometrical lock-up, and more complex self-contacting situations, are given by Przybyl & Pieranski (1998). For related problems of optimal and ideal forms, and best packing, see Stasiak, *et al*, (1998), Maritan, *et al*, (2000) and Stasiak & Maddocks (2000).

8. Solution of the uniform loaded ply

We have seen in the results of Coleman & Swigon (2000) that many long plies are approximately uniform. So we now use our general formulation to derive the load deflection characteristics of a *ULP* subjected to an end wrench (G, N). Each rod in the ply has length L, and in the balanced state with $G = N = 0$ the helical angle is β. We want to find the elongation and end rotation of the ply as functions of G and N, these being the 'corresponding displacements' through which G and N do work. The helical angle, θ, will vary during the loading process, but we assume the end conditions are such that the ply always remains (at least approximately) uniform, with θ constant along its length.

8.1 The two corresponding displacements

We define γ as the variable length of the ply, $L\cos\theta$, divided by the radius, r. We next

define n as the total rotation (in radians) of the whole ply, measured from the datum in which the 2 rods lie straight side by side. Writing the aspect ratio $a \equiv L/r$, we have

$$g = a \cos q \tag{30}$$

$$n = a \sin q \tag{31}$$

$$g^2 + n^2 = a^2 \tag{32}$$

giving $g(q)$ and $n(q)$ subjected to the constraint of (32).

8.2 A self-contained energy analysis

With our general mechanics result (18) and the kinematic condition (6) we are already in a position to fully analyse the uniform loaded ply. However, we give here a quick and self-contained energy analysis which is instructive and illuminating: it shows the energy balances at work, when high twist is alleviated by the rod bending into a writhed configuration. A similar energy analysis for the generalised ply using the calculus of variations to minimise the potential energy with respect to $q(s)$ is given by van der Heijden, Thompson & Neukirch (2001) and is summarised here in Appendix 2.

Our right-handed *ULP* with end wrench (G, N) has one degree of freedom, q. The curvature of a helical rod is $k = \sin^2 q / r$, and as in (5) the writhe of the two rods is $Wr = -\frac{1}{2}(a/p) \sin 2q$. The twist rate, using $Lk = Tw + Wr$, is given by $t r = t_0 r + \frac{1}{2} \sin 2q$. The bending energy of the two rods, U_B, the torsional energy, U_C, and the energy of the end loads, U_L, are given by

$$U_B = \tfrac{1}{2}B2Lk^2 = (BL/r^2) \sin^4 q \tag{33}$$

$$U_C = \tfrac{1}{2}C2Lt^2 = (CL/r^2)(t_0 r + \tfrac{1}{2} \sin 2q)^2 \tag{34}$$

$$U_L = -Ggr - Nn = -GL \cos q - Na \sin q \tag{35}$$

The total potential energy is $V(q) = U_B + U_C + U_L$, and for equilibrium $\partial V/\partial q = 0$, giving

$$4\sin^3 q \cos q + 2g(t_0 r + \tfrac{1}{2} \sin 2q) \cos 2q + (Gr^2/B) \sin q - (Nr/B) \cos q = 0 \tag{36}$$

The bracketed term after g is simply $t r$, so this agrees with (18). With $G = N = 0$ and $q = b$ we have the *UBP* of Fraser and his co-workers. For given g and $t_0 r$, together with the load parameters (Gr^2/B) and (Nr/B), equation (36) can be solved for the ply angle q. Notice that the ply can be unwound (with $G = 0$) by adjusting N, until at $N = 2Ct_0$ we find $q = 0$, having returned to the a-state of the manufacturing process. Beyond this value of N, the winding of the ply will be reversed.

8.3 Energy changes in the ply

It is instructive to compare the elastic energies in the pre-ply (a) and balanced (b) states.

The strain energy in the straight twisted configuration, U_a, is found from (34) with $q = 0$ and $\tan a = t_0 r$. Meanwhile, that in the balanced state, U_b, is obtained by adding (33) and (34) with $q = b$. They are given by

$$r^2 U_a = CL \tan^2 a \approx CL\, a^2 \tag{37}$$

$$r^2 U_b = BL \sin^4 b + CL(\tan a + \tfrac{1}{2} \sin 2b)^2 \approx BLb^4 + CL(a + b)^2 \tag{38}$$

In these two formulae the approximations hold for small angles, and remembering that from (22) we have $a \approx - b$, we have

$$U_a = \text{order } a^2 \tag{39}$$

$$U_b = \text{order } a^4 \tag{40}$$

To a first approximation there is no torsional energy in the balanced state, agreeing with our observation in §7.2 that the twist is of smaller order than the link and writhe. The strain energy of the balanced ply is an order of magnitude less than that of the pre-ply. The difference in energy is equal to the work done by N in passing quasi-statically between the two states with G always zero.

8.4 Contact force in the *ULP*

A vital consideration for a loaded ply is the sign of the contact force. The expression for the force/arclength can be written, using results of §5.4 and (7) and (11) as

$$pr^3 = \sin q \tan q \ (B \sin^2 q \cos q - Ct\, r \sin q + \tfrac{1}{2} Gr^2) \tag{41}$$

As a limit to the range of physically permissible configurations, we shall be particularly interested in the vanishing of p, for which

$$Gr^2/B = \sin q \ (2gt\, r - \sin 2q) = \sin q \ [\, 2gt_0 r + \sin 2q\, (g - 1)\,] \tag{42}$$

where the second equation in terms of t_0 is obtained using (6). If we eliminate q between (36) and (42) we find the locus of $p = 0$ shown in the control space of fig 10. Crossing this line as we move away from the origin where $G = N = 0$ and p is positive, the results become unphysical because they imply a negative contact pressure between the rods. A second limit, relevant when $G < 0$ with the ply under compression, corresponds to Euler buckling of the ply. However, we are mainly concerned with a very long ply (which can effectively carry no compression) so we do not examine this limit here.

8.5 Nonlinear constitutive relationships

The nonlinear constitutive relationships for the *ULP*, represented by (36), are nicely displayed by drawing the straight lines corresponding to a sequence of fixed q values in the non-dimensional control space of (Nr/B) against (Gr^2/B) as in fig 10. Here, the angle between a line and the positive Gr^2/B axis gives directly the angle q which varies in equal

increments from -45° to +45°. Imagining q to be plotted vertically out of the paper, the lines are the contours of an equilibrium response surface which exhibits a fold. The upper part of the surface above the fold (including, for example, the regime of positive *N*, *G* and q) is stable, while the lower part is unstable. Physically permissible regimes, with positive contact pressure, are denoted by solid lines. These are separated from the unphysical broken lines by the trajectory of $p = 0$ which passes through the pre-ply a-state (solid circle) through which passes a horizontal line with $q = 0$. The balanced state at the origin with $q = b$ is shown as an open circle. Notice that the fold can be reached from the b-state by suitable control changes, without *p* becoming negative. The parameters of this figure are $t_0 r = -1.5$, with an initial stripe angle of $y_a = -56°$, and $g = 1.25$. The latter is within the experiment range for DNA, but note that it corresponds to a solid circular rod of Poisson's ratio $n = -0.2$. The variation of *n* with (Gr^2/B) in the absence of any applied moment ($N = 0$) is compared with an experimental study in §8.7.

8.6 Linear constitutive relationships

With g, $t_0 r$ and *B* given, the governing equation of the *ULP* is (36) together with the displacements (30) and (31). To determine the linear response about the balanced state, we write these equations and their derivatives as

$$F[G, N, q] \equiv 4\sin^3 q \cos q + 2g t_0 r \cos 2q + \tfrac{1}{2} g \sin 4q + (Gr^2/B)\sin q - (Nr/B)\cos q = 0 \qquad (43)$$

$$\partial F/\partial q = -4\sin^4 q + 3\sin^2 2q - 4g t_0 r \sin 2q + 2g \cos 4q + (Gr^2/B)\cos q + (Nr/B)\sin q \qquad (44)$$

$$\partial F/\partial G = (r^2/B) \sin q \qquad (45)$$

$$\partial F/\partial N = -(r/B) \cos q \qquad (46)$$

$$g[q] = a \cos q, \quad \mathrm{d}g/\mathrm{d}q = -a \sin q \qquad (47)$$

$$n[q] = a \sin q, \quad \mathrm{d}n/\mathrm{d}q = a \cos q \qquad (48)$$

Independently specifying *G* and *N*, we can solve (43) for $q = q(G, N)$, and then (47) and (48) give *g* and *n*. Note that we cannot independently specify *g* and *n*, due to the constraint of (32). So we write

$$g = g[q(G, N)] \qquad n = n[q(G, N)] \qquad (49)$$

We want to find the linear *flexibility coefficients* (evaluated in the balanced b-state),

$$\left.\begin{array}{ll} \mathrm{d}g/\mathrm{d}G = \mathrm{d}g/\mathrm{d}q \;\; \partial q/\partial G & \mathrm{d}g/\mathrm{d}N = \mathrm{d}g/\mathrm{d}q \;\; \partial q/\partial N \\ \mathrm{d}n/\mathrm{d}G = \mathrm{d}n/\mathrm{d}q \;\; \partial q/\partial G & \mathrm{d}n/\mathrm{d}N = \mathrm{d}n/\mathrm{d}q \;\; \partial q/\partial N \end{array}\right) \qquad (50)$$

To find the required derivatives we write (43) as the formal identity

$$F[G, N, q(G, N)] \equiv 0 \qquad (51)$$

and differentiate this totally with respect to *G* and *N* as follows

$$dF/dG = \partial F/\partial G + \partial F/\partial q \;\; \partial q/\partial G \equiv 0 \tag{52}$$

$$dF/dN = \partial F/\partial N + \partial F/\partial q \;\; \partial q/\partial N \equiv 0 \tag{53}$$

giving

$$\partial q/\partial G = -\,(r^2/B)\sin q \;\; / \; \partial F/\partial q \tag{54}$$

$$\partial q/\partial N = (r/B)\cos q \;\; / \; \partial F/\partial q \tag{55}$$

The flexibility coefficients (elements of a non-diagonal *flexibility matrix*) become

$$\begin{matrix} dg/dG = (ar^2/B)\sin^2 q \;/\; \partial F/\partial q & dg/dN = -\,(ar/B)\sin q \cos q \;/\; \partial F/\partial q \\ dn/dG = -\,(ar^2/B)\sin q \cos q \;/\; \partial F/\partial q & dn/dN = (ar/B)\cos^2 q \;/\; \partial F/\partial q \end{matrix} \tag{56}$$

Evaluating (43) and (44) in the b-state with $G = N = 0$, and $q = b$, we have

$$4\sin^3 b \;\cos b \; + 2g t_0 r \cos 2b \; + \tfrac{1}{2} g \sin 4b \; = 0 \tag{57}$$

$$\partial F/\partial q \; = -4\sin^4 b + 3\sin^2 2b - 4g t_0 r \sin 2b + 2g \cos 4b \tag{58}$$

Regarding b as the measure of $t_0 r$, we can now solve (57) for $t_0 r(b)$ and substitute it into (58). Then putting (58) into (56) and evaluating at $q = b$ gives the flexibility coefficients. We shall not pursue the general problem further, but finally write down the form of the flexibility coefficients when the angle b is small as

$$\begin{matrix} (2C/Lr)dg/dG = b^2 + O(b^4) & (2C/L)dg/dN = -b + 2(9-5g)b^3/3g + O(b^5) \\ (2C/Lr)dn/dG = -b + 2(9-5g)b^3/3g + O(b^5) & (2C/L)dn/dN = 1 + 3(g-2)b^2/g + O(b^4) \end{matrix} \tag{59}$$

Note that for $b = 0$, the torsional flexibility is $dn/dN = \tfrac{1}{2} L/C$, namely half that of a single rod of length L. The other coefficients vanish with b, as they should for two straight inextensional rods. The negative signs correspond to the fact that as we pull a ply, we tend to unwind it.

8.7 Experimental verification

Results of an experiment, performed with the assistance of Ben Thompson, grandson of the first author, are shown in fig 11. A short length of ply was made from two silicone rubber rods, each of length L = 21 cm, lubricated with oil to minimise frictional forces. The diameter of the rods was 3.515 mm, and Young's Modulus of the rubber was estimated to be 1.97×10^6 N/m^2. The maximum load applied was 963 g, corresponding to Gr^2/B = 1.977. With zero applied twisting moment (N = 0) the graph shows a plot of the measured end rotation, n, against the dimensionless load parameter corresponding to the applied axial tension, G. The experimental points, denoted by solid circles, agree well with the drawn theoretical curve. The slight disagreement at high load is almost certainly due to factors not considered in the theory, such as the axial extensibility of the rubber rod, and

the Poisson contraction of its radius.

9. Assessing the link from a plasmid micrograph

We shall finally see how the theoretical results and concepts can be used to assess the link, *Lk*, of a DNA plasmid based on its micrograph image. The studies of Coleman & Swigon (2000), which include careful stability tests (Tobias *et al* 2000), show that to alleviate a high twist, a plasmid will writhe in space to form a super-coil, a common form of which is the interwound configuration with a ply and two end loops. Fig 2 shows one of their analysed configurations for which the prescribed link was $Lk = 10$ and the calculated writhe was $Wr = 7.548$. From such a photograph of an interwound plasmid, how can we best estimate its link?

9.1 Geometry of writhe in a ply

Since most of the rod is in the ply, it is tempting to use just the ply for our estimate, ignoring the length of rod in the end loops. Moreover the ply angle, θ, varies only minutely along the length, so we here assume it to be constant, with the rods in the form of a helix. The result for the writhe in two interwound helices, equation (5), then gives

$$\mathrm{Wr} = Dr^* \cos\theta = \pm 2K \cos\theta \tag{60}$$

Here $Dr^*=2K$ is the particular directional writhe corresponding to the number of signed crossings in a *side view of a (long) ply*, equal to 8 in fig 2. Now from this picture we can estimate the balanced ply angle as $\beta \approx -15°$, giving $\cos\beta = 0.965$ and our estimate for the writhe becomes $Wr \approx 7.73$. This compares well with the value of $Wr = 7.548$ computed by Coleman and Swigon.

9.2 Mechanics of twist in a ply

The geometrical arguments employed so far have been used to analyse the writhing of DNA for many years. However, now that the equations of the ply mechanics are known, these can be used to extract more information from a micrograph. As we demonstrate below, we can estimate the link as well as the writhe, just on the basis of a crossings count. Equation (14) gives us the total twist in our plasmid of length S

$$Tw\,(2\pi r\gamma/S) = \tau r\gamma = -\sin^2\beta \tan 2\beta \tag{61}$$

We now set the stiffness ratio as $\gamma = 2/3$, and the ratio of plasmid radius to rod length, r/S, equal to 4.1×10^{-3}, these being as used by Coleman & Swigon (fig 2). We have finally $Tw = +2.25$, giving via (3) our estimate for the link of the plasmid,

$$Lk = Tw + Wr = 7.73 + 2.25 = 9.98. \tag{62}$$

This is in excellent agreement with the link of 10 used by Coleman and Swigon.

10. Concluding Remarks

We have reviewed and extended recent work on the twisting and writhing of DNA

molecules, looking especially at the mechanics of supercoiling. We have made a careful physical examination of the equations governing the so-called ply in which two strands coil around one another in the form of a helix. We hope that our precise but physical approach, backed up by experimental work, will be helpful in opening up the rather esoteric subject of twisted elastic rods to a wide audience of molecular biologists.

Specifically, we have extended the variable ply formulation of Coleman and Swigon to include end loads, and the derived constitutive relations of this generalised ply are shown to be in excellent agreement with experiments. We have addressed the problem of determining the link, twist and writhe of a DNA plasmid from an inspection of its electron micrograph. Previous work has made use of topological results, but we have shown how the *kinematics* can be augmented by the *mechanics*, obtaining a very precise result in a trial calculation.

In continuation of the present work (van der Heijden *et al*, 2001) we have made a variational formulation of the generalised ply, summarised here in Appendix 2, and computed variable ply solutions with clamped ends, as illustrated here in fig 12.

References

Bouchiat, C. & Mezard, M. 1998 Elasticity model of supercoiled DNA molecule, *Phys. Rev.Lett*. **80** 1556-1559.

Calladine, C. R. 1980 Toroidal elastic supercoiling of DNA, *Biopolymers*, **19**, 1705-1713.

Calladine, C. R. & Drew, H. R. 1997 *Understanding DNA: the molecule and how it works*, Second Edition, Academic Press, San Diego.

Calugareanu, G. 1961 Sur les classes d'isotopie des noeuds tridimensionnels et leurs invariants, *Czech. Math. J.* **11**, 558-625.

Champneys, A. R. & Thompson, J. M. T. 1996 A multiplicity of localized buckling modes for twisted rod equations, *Proc. R. Soc. Lond.*, A **452**, 2467-2491.

Champneys, A. R., van der Heijden, G. H. M. & Thompson, J. M. T. 1997 Spatially complex localization after one-twist-per-wave equilibria in twisted circular rods with initial curvature, *Phil. Trans. R. Soc. Lond*., A **355**, 2151-2174.

Coleman, B. D. & Swigon, D. 2000 Theory of supercoiled elastic rings with self-contact and its application to DNA plasmids, *J. Elasticity* **60**, 173-221.

Coleman, B. D., Swigon, D. & Tobias, I. 2000 Elastic stability of DNA configurations. II Supercoiled plasmids with self-contact, *Phys. Rev. E* **61**, 759-770.

Fraser, W. B. & Stump, D. M. 1998 The equilibrium of the convergence point in two-strand yard plying, *Int. J. Solids Structures* **35** 285-298.

Fuller, F. B. 1971 The writhing number of a space curve, *Proc. Natl. Acad. Sci. USA.* **68**, 815-819.

Fuller, F. B. 1978 Decomposition of the linking of a closed ribbon: a problem from molecular biology, *Proc. Natl. Acad. Sci. USA.* **75**, 3557-3561.

Goriely, A. & Tabor, M. 1998 Nonlinear dynamics of filaments. IV Spontaneous looping of twisted elastic rods, *Proc. R. Soc. Lond.* A **454** 3183-3202.

Heath, P. J., Clendenning, J. B., Fujimoto, B. S. and Schurr, J. M. 1996 Effect of bending strain on the torsion elastic constant of DNA, *J. Mol. Biol.* **260** 718-730.

Horowitz, D. S. & Wang, J. C. 1984 Torsional rigidity of DNA and length dependence of the free energy of DNA supercoiling, *J. Mol. Biol.* **173** 75-91.

Manning, R. S. & Maddocks, J. H. 1999 Symmetry breaking and the twisted ring,

Comput. Methods Appl. Mech. Engrg **170** 313-330.
Manning, R. S., Maddocks J. H. & Kahn, J. D. 1996 A continuum rod model of sequence-dependent DNA structure, *J. Chem. Phys.* **105** 5626-5646.
Maritan, A., Micheletti, C., Trovato, A. & Banavar, J. R. 2000 Optimal shapes of compact strings, *Nature* **406** 287-290 (20 July).
Przybyl, S. & Pieranski, P. 1998 In search of ideal knots III Application of Maple V.4 to the problem of two ropes tightly twisted together, *Pro Dialog* **6** 18 (in Polish).
Stasiak, A., Katritch, V. & Kauffman, L. H. 1998 *Ideal Knots*, World Scientific, Singapore.
Stasiak, A. & Maddocks, J. H. 2000 Best packing in proteins and DNA, *Nature* **406** 251-253 (20 July).
Strick, T. R., Allemand, J. F., Bensimon, D., Bensimon, A. & Croquette, V. 1996 The elasticity of a single supercoiled DNA molecule, *Science* **271** 1835-1837.
Stump, D. M. & Fraser, W. B. 2000 Multiple solutions for writhed rods: implications for DNA supercoiling, *Proc. R. Soc. Lond.* A **456** 455-467.
Stump, D. M., Fraser, W. B. & Gates, K. E. 1998 The writhing of circular cross-section rods: undersea cables to DNA supercoils, *Proc. R. Soc. Lond.* A **454** 2123-2156.
Swigon, D. 1999 *Configurations with self-contact in the theory of the elastic rod model for DNA*, PhD Dissertation, Rutgers, State University of New Jersey, USA. January.
Thompson, J. M. T. & Champneys, A. R. 1996 From helix to localized writhing in the torsional post-buckling of elastic rods, *Proc. R. Soc. Lond.*, A **452**, 117-138.
Tobias, I., Swigon, D. & Coleman, B. D. 2000 Elastic stability of DNA configurations. I General theory, *Phys. Rev. E* **61**, 747-758.
van der Heijden, G. H. M. 2001 The static deformation of a twisted elastic rod constrained to lie on a cylinder, *Proc. R. Soc. Lond.* A **457**, 695-715.
van der Heijden, G. H. M., Champneys, A. R. & Thompson, J. M. T. 1998 The spatial complexity of localised buckling in rods with non-circular cross-section, *SIAM J. Appl. Math.,* **59**, 198-221.
van der Heijden, G. H. M., Champneys, A. R. & Thompson, J. M. T. 2002 Spatially complex localisation in twisted elastic rods constrained to a cylinder, to appear in *Int. J. Solids Structures.*
van der Heijden, G. H. M., Neukirch, S., Goss, V. G. A. & Thompson, J. M. T. 2002 Instability and self-contact phenomena in the writhing of clamped rods, to be published.
van der Heijden G. H. M. & Thompson, J. M. T. 1998 Lock-on to tape-like behaviour in the
torsional buckling of anisotropic rods, *Physica D*, **112**, 201-224.
van der Heijden, G. H. M. & Thompson, J. M. T. 2000 Helical and localised buckling in twisted rods: a unified analysis of the symmetric case, *Nonlinear Dynamics* **21**, 71-99.
van der Heijden, G. H. M., Thompson, J. M. T. & Neukirch, S. 2001 A variational approach to loaded ply structures, submitted to *J. Vibration & Control*.
White, J. H. 1969 Self-linking and the Gauss integral in higher dimensions, *Am. J. Math.* **91**, 693-728.
Zajac, E. E. 1962 Stability of two planar loop elasticas, *J. Appl. Mech.* **29** 136-142.

Appendix 1 Notation

a	aspect ratio of rod, $a \equiv L/r$ (see §8.1).
A	angle given to the ends of the two rods when making a ply (see §4.1).
B, C	bending and torsional stiffnesses of a rod (see §2).
Dr	directional writhe, with $Wr = < Dr >$ (see §3.4).
Dr^*	Value of Dr in a special side view (see §9.1).
F	a force arising from the decomposition of T and V (see §5.2).
g	non-dimensional length of ply made from two rods of length L (see §8.1).
G, N	applied tension and moment (tightening) on a loaded ply (see 5.1).
K	number of helical waves in one rod, given by $K = L \sin q /2p\, r$ (see §4.3).
Lk, Tw, Wr	link (turns), total twist (turns), writhe. Related by $Lk = Tw + Wr$ (see §3.3).
M_P, M_N	transmitted moments in a rod (see §5.3).
M_F, M_A	moments arising from decomposition of M_P (see §5.5).
n	total rotation in radians of the ply, zero when rods are straight (see §8.1).
r, L	radius and length, of circular rod modelling a strand of DNA (see §3.1).
s, t	arc-length and time, t, which replaces s in the dynamic analogy (see §5.1).
T, U, V	transmitted tension and shears in a rod (see §5.2).
U_B, U_C, U_L	bending energy, torsional energy and energy of the end loads (see §8.2).
b	value of q in the uniform b-state, saddle of the variable ply (see §5.7).
g	ratio of stiffnesses, $g \equiv C/B$. For DNA we have $0.7<g<1.5$ (see §2).
$q(s)$	helical angle of the ply, zero for two straight rods (see §5.1).
k	curvature of a helical rod, $k = \sin^2 q /r$ (see §8.2).
δl	a small deformation angle (see fig 5).
n	Poisson's ratio of a solid circular rod, with $g = C/B = 1/(1+n)$ (see §2).
t	right-handed twist rate in a rod, in radians per unit length (see §3.2).
t_0	initial t put into each rod in the making of a ply (see §4.1).
f	end rotation of a rod (see §3.2).
y	stripe angle of a marked rod, $\tan y = t\, r$ (see §3.2).
y_a, y_b	values of y in the straight a-state and the balanced b-state (see §7.1).

Appendix 2 Variational Formulation of the Generalised Ply

In more recent work, van der Heijden *et al* (2001) show how a variational approach offers an elegant derivation of the differential equation of the loaded non-uniform ply, and we give here a brief synopsis. In place of (33) to (35), the total potential energy of the generalised ply is

$$V = 2\int_0^L (\frac{1}{2} Bk^2 + \frac{1}{2} Ct^2)\, ds - Ggr - Nn\,.$$

With q measuring the deviation of the tangent vector from the ply axis, and f representing the internal twist, the total curvature, twist and potential energy can be written as

$$k^2 = q'^2 + \frac{1}{r^2}\sin^4 q \qquad t = f' + \frac{1}{r}\sin q \cos q \qquad V = \int_0^L \Psi(q, q', f, f')\, ds$$

where Ψ is the known integrand of V. The Euler-Lagrange equations are

$$\frac{d}{ds}\frac{\partial \Psi}{\partial q'} = \frac{\partial \Psi}{\partial q} \qquad\qquad \frac{d}{ds}\frac{\partial \Psi}{\partial f'} = \frac{\partial \Psi}{\partial f}$$

Since Ψ is independent of f the latter is an *ignorable* variable and the second equation proves t = const. The first equation gives our differential equation (12) for the loaded variable ply.

Figure Captions

Figure 1 This photograph shows a rubber rod forming a left-handed variable balanced ply (*VBP*) with one free end loop. The helical angle varies along the ply, and at the right-hand end we see the *VBP-skip-fly* phenomenon, discovered by Coleman and Swigon (2001).

Figure 2 A left-handed variable balanced ply with end loops analysed and drawn by Coleman & Swigon (2001). The prescribed link was *Lk* =10, the derived writhe was *Wr* = 7.548.

Figure 3 Sign convention for directional writhe, *Dr*, and hence for writhe, *Wr* = <*Dr*>. We put continuous arrows on the curve (the original direction chosen being irrelevant) and count the *signed* crossings according to the right-hand rule as follows. Point the thumb of the right hand along the top arrow, and if the curled fingers (with the back of the hand facing the page) point along the bottom arrow the sign is positive: conversely, it is negative. The sum of the *signed* crossings gives us *Dr*.

Figure 4 Making a ply from two straight twisted rods. In passing from the pre-ply a-state to the balanced b-state the link is conserved at *Lk* = -6 . This negative link creates a right-handed ply.

Figure 5 Forces and moments acting in a right-handed generalised ply (*GP*) with variable helical angle, $q(s)$, subjected at its ends to a wrench (*G*, *N*).

Figure 6 Phase portrait of the variable balanced ply (*VBP*). The saddle fixed point, S, corresponds to the uniform balanced ply in which the helical angle, q (here in radians), is constant. The lower-right picture shows the variation of $q(s)$ along a trajectory that passes close to S, illustrating the 'boundary layer' effect.

Figure 7 A sequence of super-coiled DNA plasmids under controlled link as analysed and drawn by Coleman & Swigon (2001). The right-hand diagram shows clearly the *VBP-skip-fly* phenomenon. The analysis is for a diameter to length ratio of 8.2×10^{-3}, corresponding to DNA of diameter 20 Å with 718 base pairs. Stiffness ratio is g = 2/3, corresponding to n = ½.

Figure 8 Continuation of fig 7 to higher *Wr*. Also shown is the variation of q at the centre of the ply, and the range of q within the ply (angles in degrees). Note that $q(s)$ takes its maximum value at the centre of the ply.

Figure 9 The first diagram compares the link-writhe graph for closed plasmids (top solid curve) due to Coleman and Swigon (2001) to that for a uniform balanced ply (lower solid curve). The second shows the extension of the uniform ply graph to higher writhe. In each

diagram the straight dashed line corresponds to $Lk = Wr$, where $Tw = 0$. The vertical line is the asymptote at Wr^*.

Figure 10 Straight lines of constant q in the control space of end-moment versus end-tension for a *ULP*. Physically permissible regimes with positive contact pressure are shown by solid lines. The pre-ply a-state is shown as a solid circle. The balanced b-state at $G=N=0$, with $q = b$, is shown as an open circle. Parameter values: $t_0 r = -1.5$, $g = 1.25$.

Figure 11 Experimental and theoretical results for a uniform ply under tension. Experimental results due to Ben Thompson are shown as solid black circles. The corresponding theoretical result is shown as a continuous curve.

Figure 12 A balanced variable ply satisfying the clamped boundary conditions implied by the moulding of §4.1. This solution is taken from van der Heijden *et al* (2001).

Super-Coiling of DNA Plasmids: Mechanics of the Generalised Ply

J. M. T. Thompson, G. H. M. van der Heijden & S. Neukirch

Centre for Nonlinear Dynamics, Civil Engineering Building,
University College London, Gower Street, London, WC1E 6BT

Set of 12 figures

(DNA Revised figs BFF)

THESE FIGS (& some short captions) ARE FOR BOOK-KEEPING PURPOSES ONLY

NEITHER FIGURES NOR CAPTIONS SHOULD BE USED FOR PUBLISHING

TOP COPIES OF THE FIGURES ARE SUPPLIED SEPARATELY

COMPLETE CAPTIONS FOR PUBLICATION ARE AT THE END OF THE MANUSCRIPT

Figure 1

F:555+

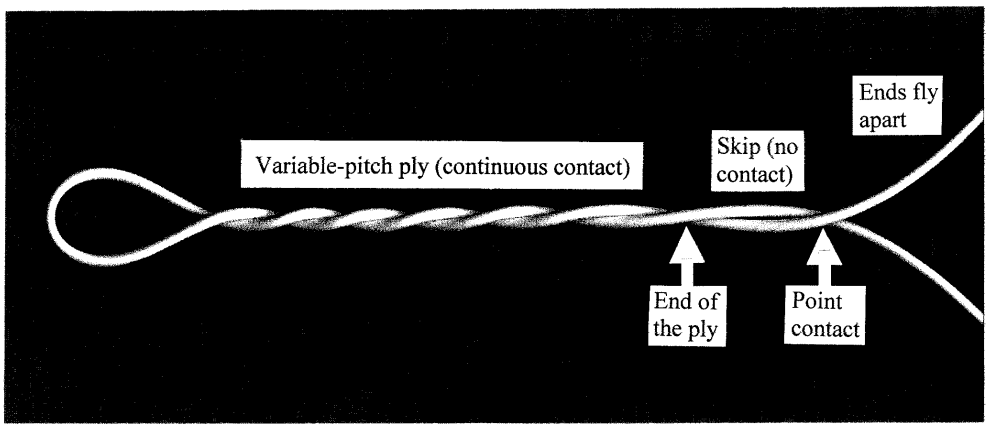

This photograph shows a rubber rod forming a left-handed variable balanced ply (*VBP*) with one free end loop. The pitch angle varies along the ply, and at the right-hand end we see the *VBP-skip-fly* phenomenon, discovered by Coleman and Swigon (2001).

Figure 2

F:566+

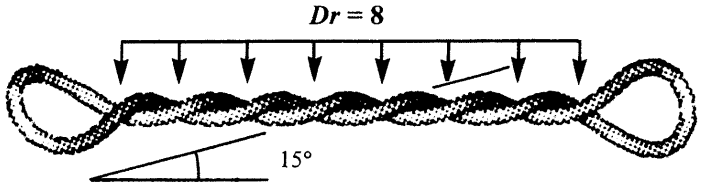

A left-handed variable balanced ply (*VBP*) with end loops analysed and drawn by Coleman & Swigon (2001). The prescribed link was Lk =10, the derived writhe was Wr = 7.548.

Figure 3

F:567++

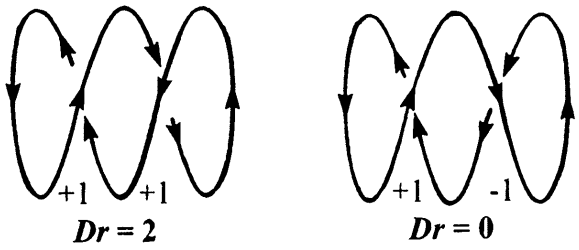

Sign convention for directional writhe, *Dr*, and hence for writhe, $Wr = < Dr >$. Put continuous arrows on the curve, the original direction chosen being irrelevant. Count the *signed* crossings according to the right-hand rule as follows. Point the thumb of the right hand along the top arrow, and if the curled fingers point along the bottom arrow the sign is positive: conversely, it is negative. The sum of the *signed* crossings gives us *Dr*.

Figure 4

F:578

α-state	Lk = -6	Tw = -6	Wr = 0	θ = 0°	ψ = -31°

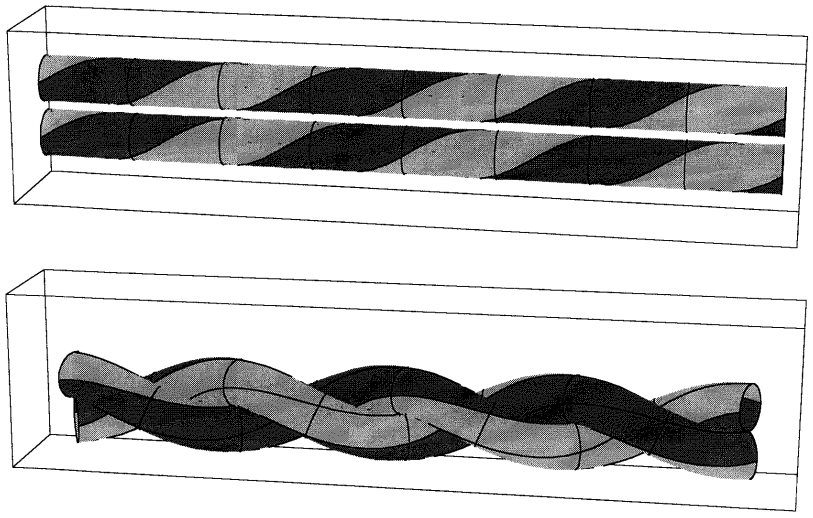

β-state	Lk = -6	Tw = -2.35	Wr = -3.65	θ = 23.4°	ψ = -13.2°

Figure 5

F:558+

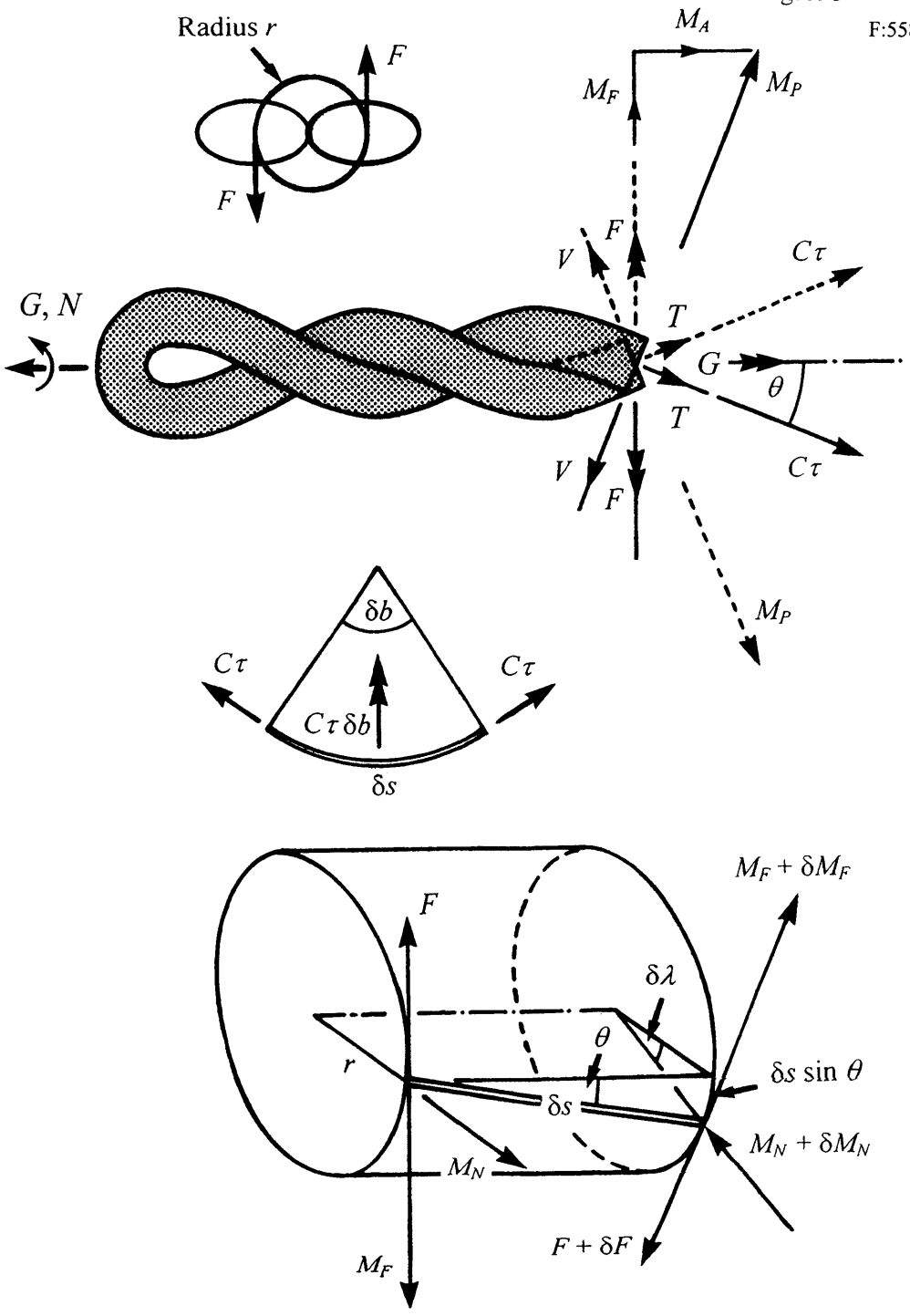

Forces and moments acting in a right-handed generalised ply (*GP*) with variable pitch angle, $\theta(s)$, subjected at its ends to a wrench (G, N).

Figure 6

F:569+

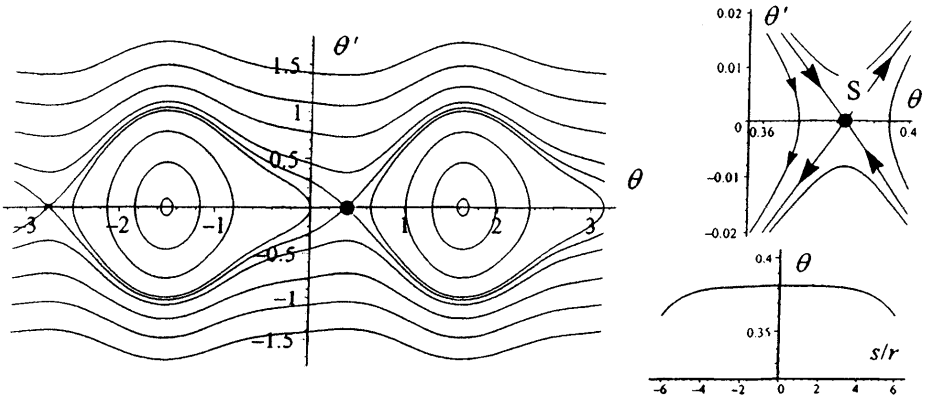

Phase portrait of the variable balanced ply (*VBP*). The saddle fixed point, S, corresponds to the uniform balanced ply in which the pitch angle, θ, is constant. The lower-right picture shows the variation of $\theta(s)$ along a trajectory that passes close to S, illustrating the 'boundary layer' effect.

Figure 7

F:544+

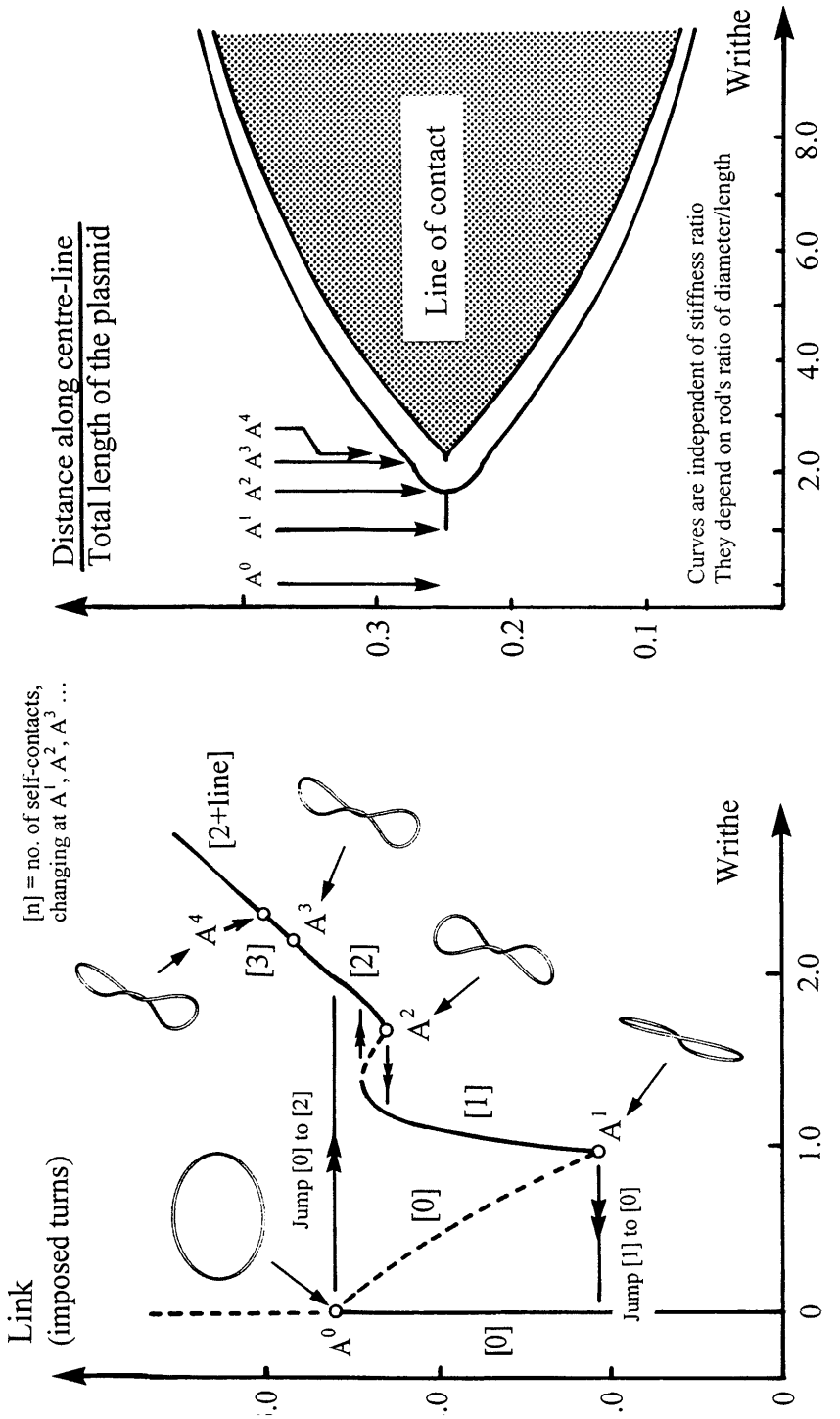

Figure 8 F:548

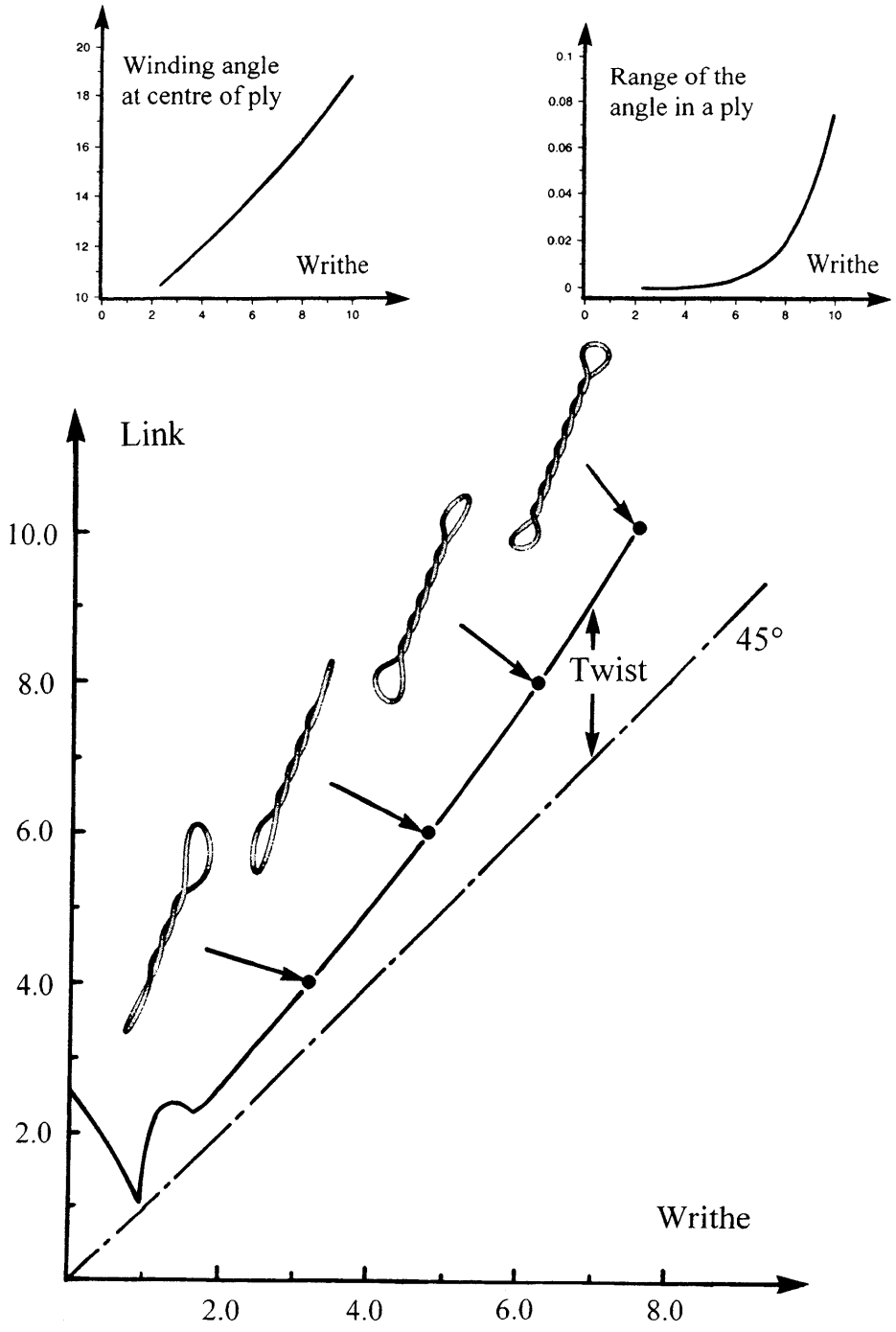

Figure 9

F : 579

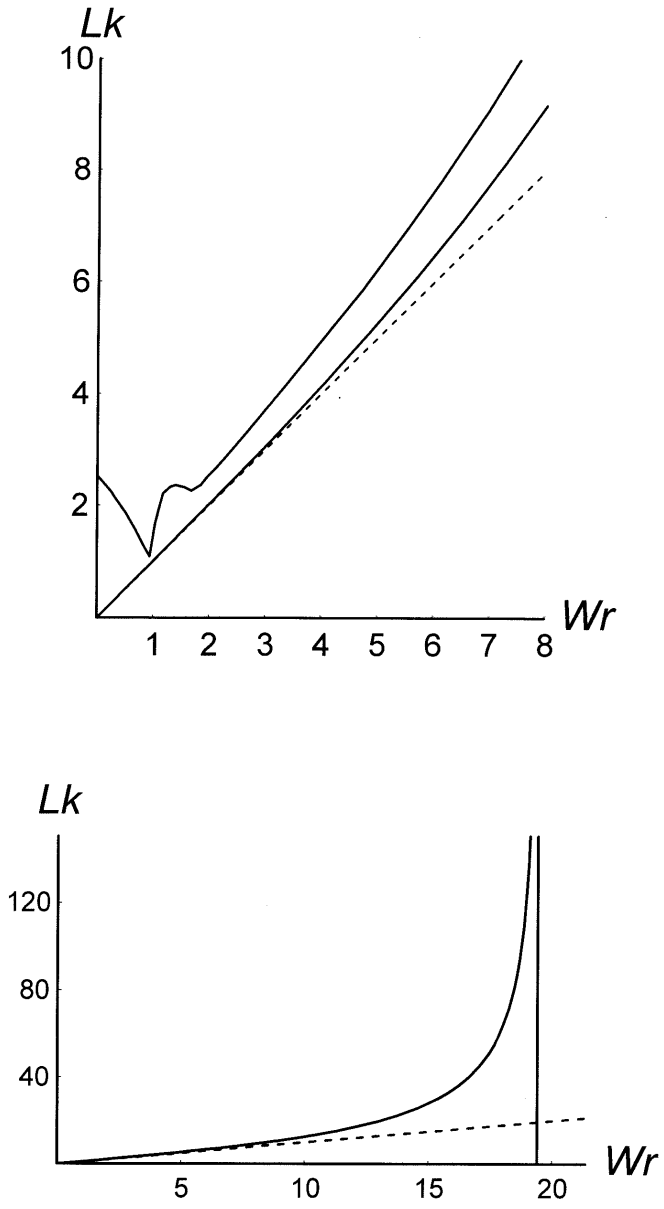

The first diagram compares the link-writhe graph for closed plasmids (top solid curve) due to Coleman and Swigon (2001) to the graph for a uniform balanced ply (lower solid curve). The second shows the extension of the uniform ply graph to higher values of the writhe. In each diagram the straight dashed line corresponds to $Lk = Wr$, where the twist is zero ($Tw = 0$).

Figure 10

F:580

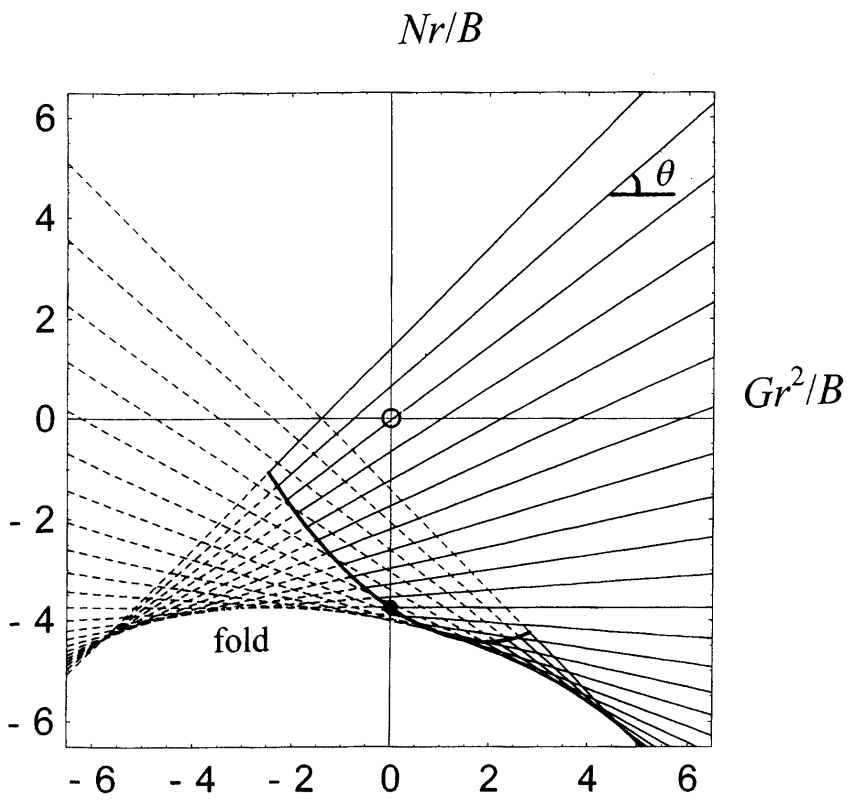

Straight lines of constant ply angle, θ, in the non-dimensional control space of end-moment, Nr/B, versus end-tension, Gr^2/B, for a uniform loaded ply. The angle between a line and the positive Gr^2/B axis gives directly the angle θ which varies in equal increments from -45° to +45°. Imagining θ to be plotted vertically out of the paper, the lines are the contours of an equilibrium response surface which exhibits a fold as shown. The upper part of the surface above the fold (including, for example, the regime of positive N, G and θ) is stable, while the lower part is unstable. Physically permissible regimes, where the contact pressure between the rods is positive, are denoted by solid lines. These are separated from the unphysical broken lines by the trajectory of $p = 0$ which passes through the pre-ply α-state (solid circle) through which passes a horizontal line with $\theta = 0$. The balanced β-state at the origin with $\theta = \beta$ is shown as an open circle. Notice that the fold can be reached from the β-state by suitable control changes, without p becoming negative. Parameter values: $\tau_0 r = -1.5$, $\gamma = 1.25$.

Figure 11

F:564 +

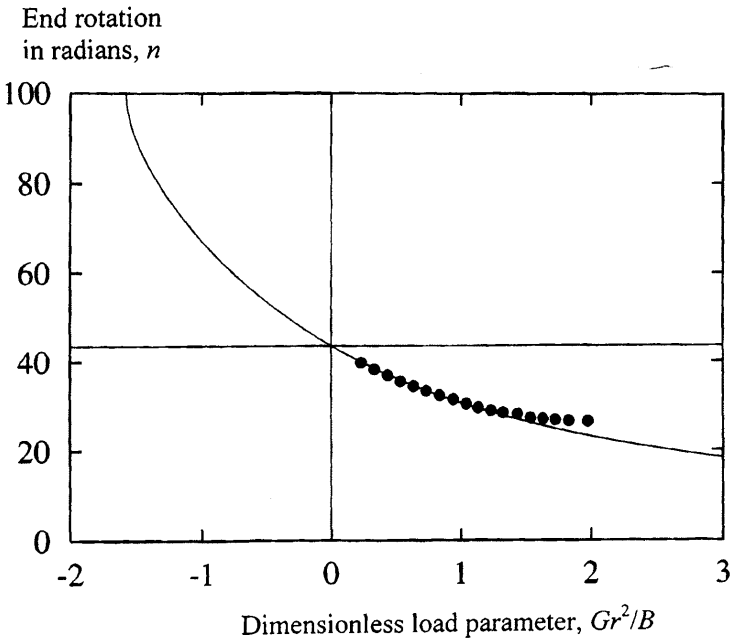

Figure 12

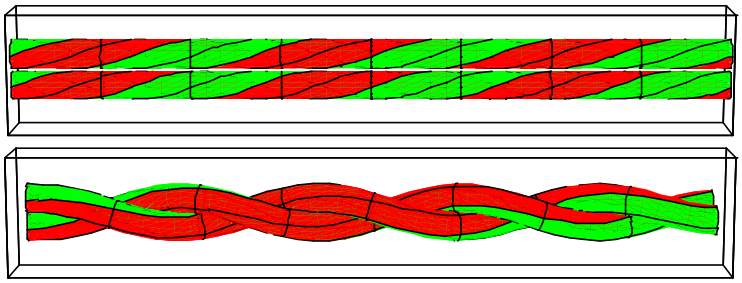

F582 BF

DNA Revised figs BFF